

Performance of Topological Insulator Interconnects

Timothy M. Philip, *Student Member, IEEE*, Mark R. Hirsbrunner, Moon Jip Park,
and Matthew J. Gilbert, *Member, IEEE*

Abstract—The poor performance of copper interconnects at the nanometer scale calls for new material solutions for continued scaling of integrated circuits. We propose the use of three dimensional time-reversal-invariant topological insulators (TIs), which host backscattering-protected surface states, for this purpose. Using semiclassical methods, we demonstrate that nanoscale TI interconnects have a resistance 1-3 orders of magnitude lower than copper interconnects and graphene nanoribbons at the nanometer scale. We use the nonequilibrium Green function (NEGF) formalism to measure the change in conductance of nanoscale TI and metal interconnects caused by the presence of impurity disorder. We show that metal interconnects suffer a resistance increase, relative to the clean limit, in excess of 500% due to disorder while the TI’s surface states increase less than 35% in the same regime.

Index Terms—Topological Insulators, Interconnects, Non-Equilibrium Green Functions (NEGF)

I. INTRODUCTION

ELECTRONIC packaging is constantly evolving in order to achieve the lower power consumption and reduced circuit delays demanded by the scaling of microelectronic circuits. Copper is an effective solution for technology nodes in the near future, but finite-size effects in metals increase copper interconnect resistivity dramatically as dimensions decrease to the nanoscale [1]. By 2025, Metal 1 pitch is predicted to reach tens of nanometers [2], where increased line edge roughness and grain boundary scattering in copper raise resistivity, and thus dissipation and signal delay, to unacceptable values [3], [4]. A materials change will hence be necessary to avoid the “interconnect bottleneck” [5], [6], whereby the poor performance of nanoscale interconnects inhibits further scaling.

Zigzag graphene nanoribbons (GNRs) have been proposed as next generation interconnect materials because of their high electron mobility [7]. Unfortunately, reliable fabrication of GNRs is difficult due to defects in growth and line edge roughness, both of which increase scattering and degrade electron mobility [8], [9]. In addition, finite-width GNRs develop a band gap [9]–[11], further reducing their conductance.

We propose the use of time-reversal-invariant topological insulators (TIs) for use in nanoscale interconnects. Topological insulators are a recently discovered class of materials that are gapped in their bulk spectrum but have surfaces that host massless, metallic Dirac fermions [12]. Time-reversal symmetry protects TI surface states from backscattering caused by charged disorder and edges, resulting in high conductance even

in the presence of these scattering mechanisms. Therefore, TI interconnects will not suffer as much as copper interconnects and GNRs from scaling-induced resistance increases.

In this letter, we investigate the transport properties of metals, GNRs, and TIs to benchmark these materials for future nanoscale interconnects. We theoretically demonstrate that below 6 nm, TI interconnect resistance is multiple orders of magnitude lower than the resistances of copper interconnects and GNRs due to the TI’s backscattering protection. Using the non-equilibrium Green function (NEGF) formalism, we show that metal interconnects greatly increase in resistance with scaling-induced disorder, while transport through TI interconnects is comparatively insensitive. Having shown that TI interconnects continue to conduct well at the nanoscale while GNRs and copper do not, we conclude that TIs are excellent candidates for a future interconnect material.

II. SEMICLASSICAL TRANSPORT

Although the widths of interconnects are decreasing, their lengths are often longer than the mean free path (MFP) of electrons and, as such, semiclassical calculations provide a useful picture of longitudinal transport [13]. We use Matthiessen’s rule to calculate the conductance of the TI Bi_2Se_3 and GNRs, assuming that all scattering mechanisms are independent of each other [14]. We consider Bi_2Se_3 because it is the most practical candidate for engineering purposes due to its bulk band gap of 0.3 eV [12]. Under Matthiessen’s rule, the conductance is given by

$$G = G_0 \sum_n \frac{1}{1 + L(\Lambda^{-1} + \ell_n^{-1})}, \quad (1)$$

where G_0 is the conductance quantum, L is the length of the wire, and Λ is the experimentally measured, room temperature MFP. In this work, we use an MFP of $1 \mu\text{m}$ for GNRs [7] and two MFPs of 10 nm and 100 nm for Bi_2Se_3 [15], [16]. The edge scattering length ℓ_n in (1) is the distance that the n th transverse mode travels before scattering off an edge and is calculated from a modified form of the equation in [17]:

$$\ell_n = W \sqrt{\frac{E_F^2 - E_g(W)^2}{(2\pi\hbar v_F n / 2W)^2} - 1}. \quad (2)$$

Here, W is the width of the wire, E_F is the Fermi energy, $E_g(W)$ is the width-dependent band gap of the material, \hbar is the reduced Planck constant, and v_F is the Fermi velocity. The modification in (2) accounts for the band gap observed in both narrow GNRs and the surface states of thin Bi_2Se_3 [9], [11]. We use experimentally observed Fermi levels of 0.26 eV and 0.21 eV for Bi_2Se_3 and GNR, respectively [12], [18]. Because the topological surface states of Bi_2Se_3 are insensitive

T. M. Philip, M. R. Hirsbrunner, and M. J. Gilbert are with the Department of Electrical and Computer Engineering, University of Illinois at Urbana-Champaign, Urbana, IL, 61802 USA (email: tphilip3@illinois.edu).

M. R. Hirsbrunner and M. J. Park are with the Department of Physics, University of Illinois at Urbana-Champaign, Urbana, IL, 61802 USA.

Manuscript received July 22, 2016; revised November 1, 2016.

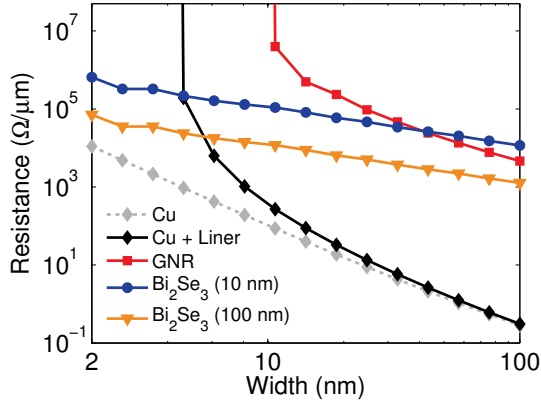


Fig. 1. The resistance of metallic GNRs, the TI Bi_2Se_3 with MFPs of 10 nm and 100 nm, and copper with and without a diffusion liner, each as a function of line width. Pure copper is the least resistive, but a required diffusion liner for manufacturing compatibility causes an resistance increase when included in line width. For widths greater than 6 nm, copper with liner has a lower resistance than Bi_2Se_3 and GNRs. Below a width of 6 nm, the resistances of Bi_2Se_3 are significantly lower than both copper with liner and the GNR, regardless of the MFP. Copper's resistance rapidly grows due to the increased grain boundary and surface scattering, while GNRs suffer from high resistance due to the increasing band gap in small-width ribbons.

to scattering off crystalline edges [19], [20], we exclude the ℓ_n term from its calculation. Additionally, the one-dimensional $n = 0$ edge mode in GNRs is susceptible to weak localization making it nonconducting [21], thus we begin the sum in (1) at $n = 1$ for GNRs. We model the resistance of copper using a combined Fuchs-Sondheimer [22] and Mayadas-Shatzkes [23] model for wires of aspect ratio 2 [3] to accurately capture both sidewall reflections and grain boundary scattering [1], resulting in values that agree well with experiments [24]. The integration of copper into CMOS manufacturing requires a diffusion barrier of a minimum width of 2 nm [3]. In order to account for the liner in copper interconnects, we also calculate resistance where the line width includes the total added liner width of 4 nm. Since the diffusion coefficients for bismuth and selenium are orders of magnitude smaller than that of copper, it does not require a diffusion barrier for Bi_2Se_3 [25]–[27].

Fig. 1 illustrates that the lower resistance of pure copper makes it the optimal material for interconnects, but accounting for the required 2 nm diffusion liner shows it to be highly resistive below a physical interconnect width of 6 nm. Above 6 nm, surface scattering is insignificant, resulting in copper's high conductance. Despite having high mobilities, both GNRs and Bi_2Se_3 are far more resistive than copper at this scale because their conductances are limited by their two-dimensional density of states. The especially poor performance of GNRs below 40 nm is caused by the lack of an $n = 0$ mode, which, combined with their band gap, significantly reduces the number of conduction channels and dramatically increases their resistance. Below 6 nm, the resistance of copper increases rapidly, attributable to increased surface scattering [24]. We see that Bi_2Se_3 with either MFP clearly outperforms copper and GNRs at this scale because it does not require a diffusion liner and has no edge scattering.

III. INFLUENCE OF DISORDER

While Matthiessen's rule is useful for longer wires, we require a quantum description for interconnect lengths below the MFP, where impurity-induced weak localization has a strong deleterious effect on conductance [28]. We employ the NEGF formalism to understand the transport properties of materials below the MFP in the presence of disorder-induced, phase-coherent scattering. Using NEGF, we calculate the percent increase in resistance, relative to the clean limit, of both TI and metal interconnects as a function of impurity disorder strength. Although copper nanowires have been shown to have highly anisotropic conductance [29], [30], the resistance change due to uniform disorder is independent of direction [31], and thus we do not consider anisotropy here. We use TI and metal models that accurately display the qualitative transport characteristics of Bi_2Se_3 and copper but do not consider GNRs because of their previously demonstrated insulating behavior at the nanoscale.

We use a Hamiltonian that accurately models the low energy behavior of TIs on a cubic lattice, defined by [32]–[34]

$$H_{\text{TI}} = \sum_{\mathbf{r}, \delta} \psi_{\mathbf{r}}^\dagger (H_m + d_{\mathbf{r}} I_4) \psi_{\mathbf{r}} + (\psi_{\mathbf{r}}^\dagger H_{\delta} \psi_{\mathbf{r}+\delta} + \text{H.c.}), \quad (3)$$

$$H_m = M\Gamma^0, \quad H_{\delta} = \frac{b\Gamma^0 + i\gamma \delta \cdot \Gamma}{2a^2}.$$

The annihilation operator $\psi_{\mathbf{r}}$ is a spinor with two orbital and two spin degrees of freedom. The vectors $\delta = (\pm a \hat{x}, \pm a \hat{y}, \pm a \hat{z})$ are the distances between nearest neighbor atoms on the lattice, spaced by the lattice constant $a = 3 \text{ \AA}$. The matrices Γ^i ($i \in \{0, x, y, z\}$) are the Dirac gamma matrices, $\Gamma = (\Gamma^x \hat{x}, \Gamma^y \hat{y}, \Gamma^z \hat{z})$, I_4 is the 4×4 identity matrix, and $M = m - 3b/a^2$. In this work, we set $m = 1.5 \text{ eV}$, $b = 9 \text{ eV \AA}^2$, and $\gamma = 3 \text{ eV \AA}$ to put the insulator in the strong topological phase with a bulk band gap of 1 eV. This large band gap results in highly localized surface states that do not hybridize, allowing the simulation of smaller structures while maintaining the qualitative behavior of larger devices. In (3), $d_{\mathbf{r}}$ is the disorder potential, which is randomly distributed in the range $-D/2 \leq d_{\mathbf{r}} \leq D/2$, representing impurities introduced during growth and fabrication [35]. Conductance calculations are averaged over ten trials for each disorder strength D , where each trial has a different random disorder potential configuration. The disorder range studied, $0 \text{ eV} \leq D \leq 5 \text{ eV}$, corresponds to a surface state MFP down to 0.32 nm, using the relation $\Lambda = 12\hbar^3 v_F^3 / (a^2 D^2 E_F)$ [36], covering the range of experimentally measured MFPs in TIs [15], [16]. The metal is modeled by a 3D tight-binding Hamiltonian with nearest-neighbor hopping $t_0 = 1.5 \text{ eV}$ [37], such that the metal has the same bandwidth as the TI. The chemical potential is set to 0.8 eV, although qualitative trends are independent of specific value. Random impurity disorder is added to the metal in the same fashion as for the TI. Grain boundary scattering is not relevant here as the device dimensions are smaller than typical grain sizes. Both materials are modeled using a wire with dimensions $(10a \hat{x}, 5a \hat{y}, 5a \hat{z})$, where transport is simulated along \hat{x} with a bias of 1 mV and temperature at 300 K.

Fig. 2 shows the percent increase in resistance, relative to the clean limit, of each interconnect versus disorder strength.

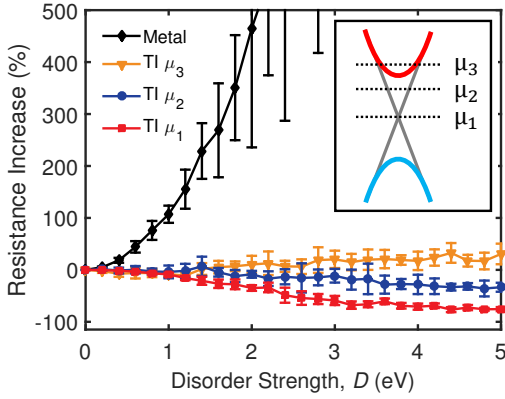


Fig. 2. Percent increase in resistance, relative to the clean limit, of a metal and a TI with chemical potentials $\mu_1 = 0$, $\mu_2 = 0.3$ eV, and $\mu_3 = 0.6$ eV as a function of disorder, simulated using NEGF. Conductance is averaged over ten trials, each using a different random disorder potential configuration. The inset graphic depicts the TI's band structure and the different chemical potentials used, denoted with dotted horizontal lines. Because of the symmetry protection of the TI's surface states, there is little change in the TI's resistance, relative to the metal's. The metal's resistance increases immediately, quickly becoming an insulator.

For the metal interconnect, on-site impurity disorder increases elastic scattering, resulting in more than a 450% increase in resistance above 2 eV of disorder. We plot the resistance of the TI at three different chemical potentials (μ_1 , μ_2 and μ_3), illustrated by the inset of Fig. 2. For conduction through the Dirac point at μ_1 , the presence of disorder decreases resistance by 76% at $D = 5$ eV. Disorder-induced mid-gap states increase the number of conduction channels, as is evident in Figure 3, resulting in the TI transitioning into a diffusive metal phase [38]–[40]. Transport at μ_2 , crossing solely through the TI surface states, results in a slight decrease in resistance as transport occurs at higher energies than most of the disorder-induced mid-gap states. The small change in resistance for the TI at μ_1 and μ_2 compared to the dramatic rise for the metal demonstrates the benefit of the topological protection of the TI surface states. Chemical potential μ_3 crosses both the surface states and the bulk bands, which results in the resistance increasing by 30% at $D = 5$ eV due to the localization of the unprotected bulk electrons. Continued conduction through the surface states, however, limits the resistance increase in the TI. Because the Fermi level of as-grown Bi_2Se_3 crosses both the bulk and surface bands [12], our calculations at μ_3 are of particular interest as they indicate that Bi_2Se_3 can benefit from both bulk conductance and surface backscattering protection.

IV. ADDITIONAL CONSIDERATIONS

Recent theoretical work suggests that inelastic scattering by acoustic phonons greatly reduces the mobility of TIs [41]. Although this is true for long lengths, TI interconnects with lengths less than or equal to the MFP may not suffer such a large degradation. To investigate inelastic scattering, we add a phenomenological on-site self-energy to the TI Hamiltonian. The scattering self-energy $\Sigma_S = -i\hbar/2\tau$ [37] is characterized by the mean free time $\tau = \Lambda/v_F$. Here, the MFP Λ is 23.8 nm [16] and the Fermi velocity v_F is 5×10^5 m/s [32], resulting in $\tau = 47.6$ fs and a scattering self-energy $\text{Im}\{\Sigma_S\} =$

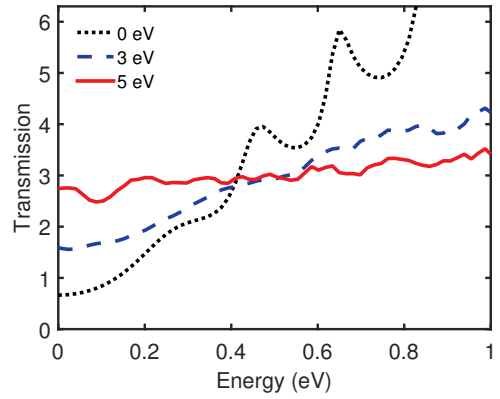


Fig. 3. The disorder-averaged transmission function of the TI interconnect for $D = 0$ eV, 3 eV, and 5 eV. Transmission is symmetric about $E = 0$ eV as a result of particle-hole symmetry in the model. As the TI transitions to a diffusive metal phase, conductive mid-gap states form, improving low energy transmission. At higher energies, however, disorder-induced weak localization continuously reduces transmission with increasing disorder, thus increasing resistance of bulk transport.

-0.014 eV. Simulated transport shows only a 20% resistance increase over that without inelastic scattering, a much smaller reduction than was reported in [41]. As such, we see that inelastic phonon scattering is not a significant source of performance degradation in nanoscale TI interconnects.

Another concern in the use of TI interconnects is that they would be in the presence of time-reversal-breaking electromagnetic fields from nearby lines, which could destroy their topological protection. We estimate the influence of this crosstalk by using Ampere's law for a wire carrying a current of 1 mA at an interconnect pitch of 5 nm resulting in a magnetic field strength $|\mathbf{B}| = 40$ mT. Such a field creates a Zeeman energy gap $E_Z = g\mu_B|\mathbf{B}|$, where $g \approx 32$ is the g -factor for Bi_2Se_3 [42] and $\mu_B = 57.9 \mu\text{eV}\cdot\text{T}$ is the Bohr magneton. Using this relation, we obtain a Zeeman energy splitting of 74.1 μeV . Therefore, even in the presence of many other lines, this gap will be smaller than 1 meV, resulting in an immeasurable impact on the TI's topological properties.

V. CONCLUSION

We have performed a numerical study to explore the use of TIs as future interconnects. Using semiclassical techniques, we find that copper is much less resistive than the Bi_2Se_3 or GNRs above line widths of 6 nm. Below this width, however, the increased surface scattering in copper and the observed band gap in GNRs cause both to rapidly rise in resistance above Bi_2Se_3 , making the TI the best candidate in this regime. Using NEGF, we also observe that disorder causes the metal's resistance to increase by orders of magnitude but has no negative impact on the TI's backscattering-protected surface states. Because TIs maintain their conductive properties under the effects of scaling microelectronics, they are excellent candidates for next-generation interconnect materials.

ACKNOWLEDGMENT

T. M. Philip and M. J. Park would like to thank Y. Kim for helpful discussions. The authors would like to thank NSF CAREER ECCS-1351871 for funding.

REFERENCES

- [1] W. Steinhogel, G. Schindler, G. Steinlesberger, M. Traving, and M. Engelhardt, "Comprehensive study of the resistivity of copper wires with lateral dimensions of 100 nm and smaller," *Journal of Applied Physics*, vol. 97, no. 2, p. 023706, 2005.
- [2] P. Kapur, J. McVittie, and K. Saraswat, "Technology and reliability constrained future copper interconnects. I. Resistance modeling," *IEEE Transactions on Electron Devices*, vol. 49, no. 4, pp. 590–597, Apr. 2002.
- [3] S. I. Association, "International Technology Roadmap for Semiconductors," 2013. [Online]. Available: <http://www.itrs.net/>
- [4] R. L. Graham, G. B. Alers, T. Mountsier, N. Shamma, S. Dhuey, S. Cabrini, R. H. Geiss, D. T. Read, and S. Peddeti, "Resistivity dominated by surface scattering in sub-50 nm Cu wires," *Applied Physics Letters*, vol. 96, no. 4, p. 042116, 2010.
- [5] C. Ababei, Y. Feng, B. Goplen, H. Mogal, T. Zhang, and K. Bazargan, "Placement and Routing in 3D Integrated Circuits," 2005.
- [6] X. Zhang and S.-C. Zhang, "Chiral interconnects based on topological insulators," in *Micro-and Nanotechnology Sensors, Systems, and Applications IV*, T. George, M. S. Islam, and A. Dutta, Eds., vol. 8373, May 2012.
- [7] K. Bolotin, K. Sikes, Z. Jiang, M. Klima, G. Fudenberg, J. Hone, P. Kim, and H. Stormer, "Ultra-high electron mobility in suspended graphene," *Solid State Communications*, vol. 146, no. 9–10, pp. 351–355, Jun. 2008.
- [8] A. Hashimoto, K. Suenaga, A. Gloter, K. Urita, and S. Iijima, "Direct evidence for atomic defects in graphene layers," *Nature*, vol. 430, no. 7002, pp. 870–3, Aug. 2004.
- [9] X. Li, X. Wang, L. Zhang, S. Lee, and H. Dai, "Chemically derived, ultrasmooth graphene nanoribbon semiconductors," *Science*, vol. 319, no. 5867, pp. 1229–1232, Feb. 2008.
- [10] Y.-W. Son, M. L. Cohen, and S. G. Louie, "Energy gaps in graphene nanoribbons," *Physical Review Letters*, vol. 97, no. 21, p. 216803, 2006.
- [11] Y. Zhang, K. He, C. Chang, and C. Song, "Crossover of the three-dimensional topological insulator Bi₂Se₃ to the two-dimensional limit," *Nature Physics*, vol. 6, no. 8, pp. 584–588, Jun. 2010.
- [12] Y. Xia, D. Qian, D. Hsieh, L. Wray, a. Pal, H. Lin, a. Bansil, D. Grauer, Y. S. Hor, R. J. Cava, and M. Z. Hasan, "Observation of a large-gap topological-insulator class with a single Dirac cone on the surface," *Nature Physics*, vol. 5, no. 6, pp. 398–402, May 2009.
- [13] Y.-M. Niquet, V.-H. Nguyen, F. Triozon, I. Duchein, O. Nier, and D. Rideau, "Quantum calculations of the carrier mobility: Methodology, Matthiessen's rule, and comparison with semi-classical approaches," *Journal of Applied Physics*, vol. 115, no. 5, p. 054512, 2014.
- [14] J. Bass, "Deviations from Matthiessen's rule," *Advances in Physics*, vol. 21, no. 91, pp. 431–604, 1972.
- [15] C. Chen, Z. Xie, Y. Feng, H. Yi, A. Liang, and S. He, "Tunable Dirac Fermion Dynamics in Topological Insulators," *Scientific Reports*, p. 1302.0123, Jan. 2013.
- [16] W. J. Wang, K. H. Gao, and Z. Q. Li, "Thickness-dependent transport channels in topological insulator Bi₂Se₃ thin films grown by magnetron sputtering," *Scientific Reports*, vol. 6, p. 25291, Apr 2016.
- [17] A. Naeemi and J. Meindl, "Conductance modeling for graphene nanoribbon (GNR) interconnects," *IEEE Electron Device Letters*, vol. 28, no. 5, pp. 428–431, 2007.
- [18] C. Berger, Z. Song, X. Li, X. Wu, N. Brown, C. Naud, D. Mayou, T. Li, J. Hass, A. N. Marchenkov, E. H. Conrad, P. N. First, and W. A. de Heer, "Electronic confinement and coherence in patterned epitaxial graphene," *Science*, vol. 312, pp. 1191–1196, 2006.
- [19] Z. Alpichshev, J. G. Analytis, J.-H. Chu, I. R. Fisher, Y. L. Chen, Z. X. Shen, A. Fang, and A. Kapitulnik, "Stm imaging of electronic waves on the surface of Bi₂Te₃: Topologically protected surface states and hexagonal warping effects," *Physical Review Letters*, vol. 104, p. 016401, Jan 2010.
- [20] Y. Takane and K.-I. Imura, "Dirac electrons on a sharply edged surface of topological insulators," *Journal of the Physical Society of Japan*, vol. 81, no. 9, p. 093705, 2012.
- [21] R. Abou-Chacra, D. Thouless, and P. Anderson, "A self-consistent theory of localization," *Journal of Physics C: Solid State Physics*, vol. 6, no. 10, p. 1734, 1973.
- [22] E. Sondheimer, *The mean free path of electrons in metals*, 1952, vol. 1, no. 1.
- [23] A. F. Mayadas and M. Shatzkes, "Electrical-resistivity model for polycrystalline films: The case of arbitrary reflection at external surfaces," *Phys. Rev. B*, vol. 1, no. 4, pp. 1382–1389, 1970.
- [24] J. M. Roberts, A. P. Kaushik, and J. S. Clarke, "Resistivity of sub-30 nm copper lines," in *2015 IEEE Int. Interconnect Technol. Conf. 2015 IEEE Mater. Adv. Met. Conf.* IEEE, May 2015, pp. 341–344.
- [25] R. N. Hall and J. H. Racette, "Diffusion and Solubility of Copper in Extrinsic and Intrinsic Germanium, Silicon, and Gallium Arsenide," *J. Appl. Phys.*, vol. 35, no. 2, p. 379, 1964.
- [26] C.-S. Kim and M. Sakata, "Diffusion Coefficient of Selenium in Silicon by Sheet Hall Coefficient Measurements," *Jpn. J. Appl. Phys.*, vol. 18, no. 2, pp. 247–254, Feb 1979.
- [27] Y. Ishikawa, Y. Kazuyuki, and I. Nakamichi, "The Diffusion of Bismuth in Silicon," *Jpn. J. Appl. Phys.*, vol. 28, no. 7, pp. 1272–1273, 1989.
- [28] P. W. Anderson, "Absence of diffusion in certain random lattices," *Physical Review*, vol. 109, pp. 1492–1505, Mar 1958.
- [29] N. Kharche, S. R. Manjari, Y. Zhou, R. E. Geer, and S. K. Nayak, "A comparative study of quantum transport properties of silver and copper nanowires using first principles calculations," *J. Phys. Condens. Matter*, vol. 23, no. 8, p. 085501, 2011.
- [30] G. Hegde, M. Povolotskyi, T. Kubis, J. Charles, and G. Klimeck, "An environment-dependent semi-empirical tight binding model suitable for electron transport in bulk metals, metal alloys, metallic interfaces, and metallic nanostructures. II. Application - Effect of quantum confinement and homogeneous strain on Cu conductance," *J. Appl. Phys.*, vol. 115, no. 12, 2014.
- [31] Q. Li, C. M. Soukoulis, I. Zambetaki, and E. N. Economou, "Localization in Highly Anisotropic Systems," *Phys. Rev. Lett.*, vol. 76, no. 19, p. 3614, 1996.
- [32] H. Zhang, C.-X. Liu, X.-L. Qi, X. Dai, Z. Fang, and S.-C. Zhang, "Topological insulators in Bi₂Se₃, Bi₂Te₃ and Sb₂Te₃ with a single Dirac cone on the surface," *Nature Physics*, vol. 5, no. 6, pp. 438–442, May 2009.
- [33] C.-X. Liu, X.-L. Qi, H. Zhang, X. Dai, Z. Fang, and S.-C. Zhang, "Model Hamiltonian for topological insulators," *Physical Review B*, vol. 82, no. 4, p. 045122, Jul. 2010.
- [34] H.-H. Hung, P. Ghaemi, T. L. Hughes, and M. J. Gilbert, "Vortex lattices in the superconducting phases of doped topological insulators and heterostructures," *Physical Review B*, vol. 87, no. 3, p. 035401, Jan. 2013.
- [35] Y. Zhu and L. Lu, *Atomistic Simulation of Quantum Transport in Nanoelectronic Devices*. Singapore: World Scientific Publishing Co., 2016.
- [36] H. Akera and T. Ando, "Theory of the hall effect in quantum wires: Effects of scattering," *Physical Review B*, vol. 41, pp. 11967–11977, Jun 1990.
- [37] S. Datta, "Nanoscale device modeling: the Green's function method," *Superlattices and Microstructures*, vol. 28, no. 4, pp. 253–278, 2000.
- [38] K. Kobayashi, T. Ohtsuki, and K.-I. Imura, "Disordered Weak and Strong Topological Insulators," *Phys. Rev. Lett.*, vol. 110, p. 236803, Jun. 2013.
- [39] B. Sbierski and P. W. Brouwer, "Z₂ phase diagram of three-dimensional disordered topological insulators via a scattering matrix approach," *Phys. Rev. B*, vol. 89, no. 15, p. 155311, Apr. 2014.
- [40] K. Kobayashi, T. Ohtsuki, K.-I. Imura, and I. F. Herbut, "Density of states scaling at the semimetal to metal transition in three dimensional topological insulators," *Phys. Rev. Lett.*, vol. 112, p. 016402, Jan 2014.
- [41] G. Gupta, M. B. A. Jalil, and G. Liang, "Evaluation of mobility in thin Bi₂Se₃ Topological Insulator for prospects of Local Electrical Interconnects," *Scientific reports*, vol. 4, p. 6838, Jan. 2014.
- [42] O. Madelung, U. Rössler, and M. Schulz, *Non-Tetrahedrally Bonded Elements and Binary Compounds I*. Springer-Verlag Berlin Heidelberg, 1998, vol. 41C.